Single-Molecule Detection

Deutsche Ausgabe: DOI: 10.1002/ange.201603038
Internationale Ausgabe: DOI: 10.1002/anie.201603038

# Direct Measurement of Single-Molecule DNA Hybridization Dynamics with Single-Base Resolution

*Gen He, Jie Li, Haina Ci, Chuanmin Qi,* and Xuefeng Guo**

***Abstract:*** *Herein, we report label-free detection of single-molecule DNA hybridization dynamics with single-base resolution. By using an electronic circuit based on point-decorated silicon nanowires as electrical probes, we directly record the folding/unfolding process of individual hairpin DNAs with sufficiently high signal-to-noise ratio and bandwidth. These measurements reveal two-level current oscillations with strong temperature dependence, enabling us to determine the thermodynamic and kinetic properties of hairpin DNA hybridization. More importantly, successive, stepwise increases and decreases in device conductance at low temperature on a microsecond timescale are successfully observed, indicating a base-by-base unfolding/folding process. The process demonstrates a kinetic zipper model for DNA hybridization/dehybridization at the single base-pair level. This measurement capability promises a label-free single-molecule approach to probe biomolecular interactions with fast dynamics.*

Deoxyribonucleic acid (DNA) acts as the molecular basis for heredity and genetics, and DNA hybridization is a fundamental process in biology. The molecular-level kinetics and functions of DNA hybridization have been extensively investigated by different single-molecule detection techniques based on optics,[1] force,[2] and electricity.[3] Although the unambiguous framework of DNA hybridization has been established, sophisticated models from single-base insights into DNA hybridization are still lacking because of limitations in either time resolution or detection capability.[4] The hairpin loop is a secondary structural motif frequently observed in DNAs and RNAs that is involved in gene expression and regulation.[5] A two-state mechanism of DNA hairpin formation, where the hairpin DNA transits between a folded base-paired state and an unfolded random-coil state with the relaxation time ranging from several microseconds to hundreds of microseconds, has been well studied as an important system of DNA hybridization using fluorescence correlation spectroscopy (FCS),[6] single-molecule fluorescence resonance energy transfer (smFRET),[7] single-molecule force spectroscopy,[8] and laser temperature jumping.[9] These studies also suggested a complicated, multistate model of fast hairpin folding, which requires experimental techniques capable of probing both long- and short-lived reaction intermediates in a wide range of detection times. One-dimensional silicon nanowires (SiNWs), whose conductance is strongly dependent on the local charge density, were shown to be high-gain field-effect sensors that are able to detect chemical or biological species in solution.[10] Recently, by rationally incorporating individual point scattering sites into SiNW field-effect transistors (FETs), we developed a direct, real-time electrical approach of sensing intermolecular interactions in biological systems with single-molecule sensitivity.[11] In this study, we take advantage of such a field-effect-based single-molecule methodology to achieve measurements of hairpin hybridization kinetics with sufficiently high signal-to-noise ratio and bandwidth that are able to reveal the dynamic folding/unfolding process of a single hairpin DNA at the single base-pair level. These measurements reveal two-level current oscillations with strong temperature dependence, which enables us to determine the thermodynamic and kinetic properties of hairpin DNA hybridization, in agreement with the results from optical methods. More importantly, we successfully observe successive, stepwise increases and decreases in device conductance at low temperature on a microsecond timescale, indicating a base-by-base unfolding/folding process. The process demonstrates a kinetic zipper model for DNA hybridization/dehybridization at the single base-pair level. This measurement capability promises a label-free single-molecule approach to probe biomolecular interactions with fast dynamics and establish biotechnologies in drug discovery,[12] DNA nanotechnology,[13] and sequencing techniques.[14]

SiNW-based single-molecule electrical biosensors (Figure 1 a) were fabricated by using a simple three-step process as described previously: SiNW FET fabrication, gap opening, and point biodecoration.[11] To ensure the reliable measurements in a buffer solution, we passivated the contact interfaces by a 50 nm-thick $SiO_2$ layer and further used photoresistant SU-8 to protect the majority of the device surface except for the conducting channel in the first step. After lithographical gap opening, the devices were immediately annealed under an octadecyltrichlorosilane (OTS) vapor in the vacuum oven to passivate the reactive hydroxy groups from the $SiO_2$ surface and avoid the trap events from

[*] G. He, J. Li, Prof. C. Qi
Key Laboratory of Radiopharmaceuticals
Ministry of Education, College of Chemistry
Beijing Normal University
Beijing 100875 (P.R. China)
E-mail: qichuanmin@bnu.edu.cn
H. Ci, Prof. X. Guo
Beijing National Laboratory for Molecular Sciences
State Key Laboratory for Structural Chemistry of Unstable and Stable Species
College of Chemistry and Molecular Engineering
Peking University
Beijing 100871 (P.R. China)
E-mail: guoxf@pku.edu.cn

Supporting information for this article can be found under: http://dx.doi.org/10.1002/anie.201603038.

  

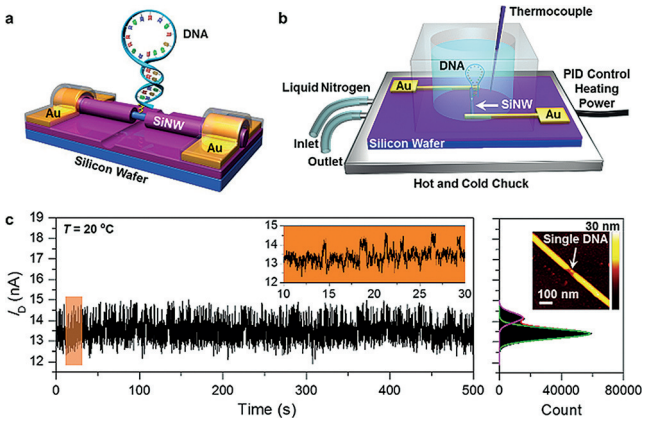


***Figure 1.*** a) Diagram of single-hairpin DNA-decorated SiNW biosensors. b) Electrical measurement setup. c) Real-time current recordings of 500 s measured in a PBS solution at $T = 20\,°C$. Inset shows representative data over a 20 s time interval. The right panel is the corresponding histogram of current values, revealing two Gaussian peaks in conductance. Inset shows an AFM image of a SiNW device, where a single hairpin DNA is attached on the sidewall.

nonspecific absorption. Then, through alkyne hydrosilylation of Si–H bonds with undecynic acid and *N*-hydroxysuccinimide (NHS)-esterification, we obtained active ester terminals for the subsequent attachment of hairpin DNAs. We finally incorporated amino-terminal hairpin DNAs at the 5′ end with five base-pairs in stem and fifteen bases in loop on the sidewall of silicon nanowires. The atomic force microscopic (AFM) image (Figure 1 c, right inset) showed a single hairpin DNA (with a height of $\approx 4.6$ nm, slightly less than the molecular length obtained from the fully-extended conformation; see the Supporting Information, Figure S4) on the side of a SiNW, indicating successful immobilization. The full method and characterization are provided in the Supporting Information.

All of the electrical measurements were carried out in PBS solution (10 mM PBS, pH 7.4). As depicted in Figure 1 b, an INSTEC hot and cold chuck was used to control the testing temperature ($\pm 0.001\,°C$), which was real-time recorded by a thermocouple. After thermally equilibrating for $\approx 10$ min, we applied a source-drain bias of 100 mV and a zero gate bias (used in all the real-time electrical measurements), and then collected the long-duration current data for at least 500 s. These measurement conditions (Supporting Information) resulted in an average input-referred noise level of $\approx 0.25$ nA, which was determined from the standard deviation of the Gaussian fits. We observed that real-time current recordings ($I$(t)) exhibited a large-amplitude two-level fluctuation at 20 °C (Figure 1 c), where the conductance distribution was well fitted into two Gaussian peaks centered at $\approx 13.41$ and $\approx 14.18$ nA, respectively. The current difference of the two states is $\approx 0.77$ nA with a signal-to-noise ratio of better than three over the flicker (1/*f*) noise background.

We carried out the measurements as a function of temperature varying from 20 °C to 65 °C with a 5 °C warming interval. Figure 2 shows a 50 s data set of a representative device (Device 1) measured at ten different temperatures and the corresponding conductance histograms. The two-level current oscillations showed a strong temperature dependence, suggesting that the conductance is mostly in the low state at low temperatures and in the high state at high temperatures. We observed this two-level fluctuating behavior in the tests of at least 10 devices. Figure S5 demonstrates another data set of Device 2, indicating that the phenomenon of the two-level current oscillation and its temperature dependence are reproducible. Control experiments, where we used a blank SiNW FET device that had been treated by hairpin DNAs after undecynic acid immobilization but was not covalently functionalized with hairpin DNAs because of the lack of essential NHS-esterification, demonstrated that the $I$(t) measurements as a function of temperature exhibited no particular fluctuations with only a Gaussian distribution that is dominated by the $1/f$ noise (Figure S6). These results eliminate the possibility of nonspecific surface absorption of either hairpin DNAs or ions in the electrolytic solution, thus confirming that the two-level current oscillations originated from the intrinsic behavior of hairpin DNAs. By calculating the areas of the two Gaussian distributions, we gained the occupations of the high and low conductance states at each temperature (Table S1) and obtained a temperature-dependent curve of the fraction of the high conductance state. This plot was in agreement with the melting curve of hairpin DNAs measured by UV/Vis absorption spectroscopy (Figure S7), with a consistent melting point ($T_m \approx 46.5\,°C$)[15] where the two states are similarly occupied. In terms of this apparent temperature correlation, we propose a model in which the fluctuation is modulated by different conformations of the hairpin DNA. Considering the fact from the melting curve that the hairpin state dominates the conformation below $T_m$ while the random-coil state dominates the conformation above $T_m$, the low-conductance state corresponds to the hairpin state and the high-conductance state corresponds to the unfolded coil state. We interpret that duplex formation and dissociation in the stem region would induce alteration of the scattering effect and/or charge transfer originated from the single defect of naked SiNWs, which results in dynamical conductivity changes of the underlying FET channel. Unlike most DNA-biosensors based on nanoscale devices at the ensemble level,[16] where the sensing principle is that negative charges from the phosphate groups electrostatically gate the conducting channel, the scattering effect at the single defect fixed on the surface of one-dimensional nanostructures is very sensitive to the change in the transmission probability at the defect. Stem duplex formation and dissociation result in the decrease and increase of the transmission probability, respectively.[3b,17]

Now that long-duration current recordings as a function of temperature reveal a two-state model of the folding/unfolding process of single-molecule hairpin DNAs where we postulate that an all-or-none transition happens between the hairpin and random coil forms, the equilibrium constant $K_m$ of duplex dissociation can be deduced according to the formula: $K_m = a/(1-a)$, where $a$ represents the fraction of the single-stranded coil state.[18] Then, we determined the thermodynamic parameters by the thermodynamic relationship, $\Delta G_m = -RT\ln(K) = \Delta H_m - T\Delta S_m$. Detailed thermodynamic results are listed in Table S1. The plot of $R\ln(K)$ to $1000/T$ shows a linear fit (Figure 3 a), giving $\Delta H_m \approx 58.28\,kJ\,mol^{-1}$ and $\Delta S_m$

  

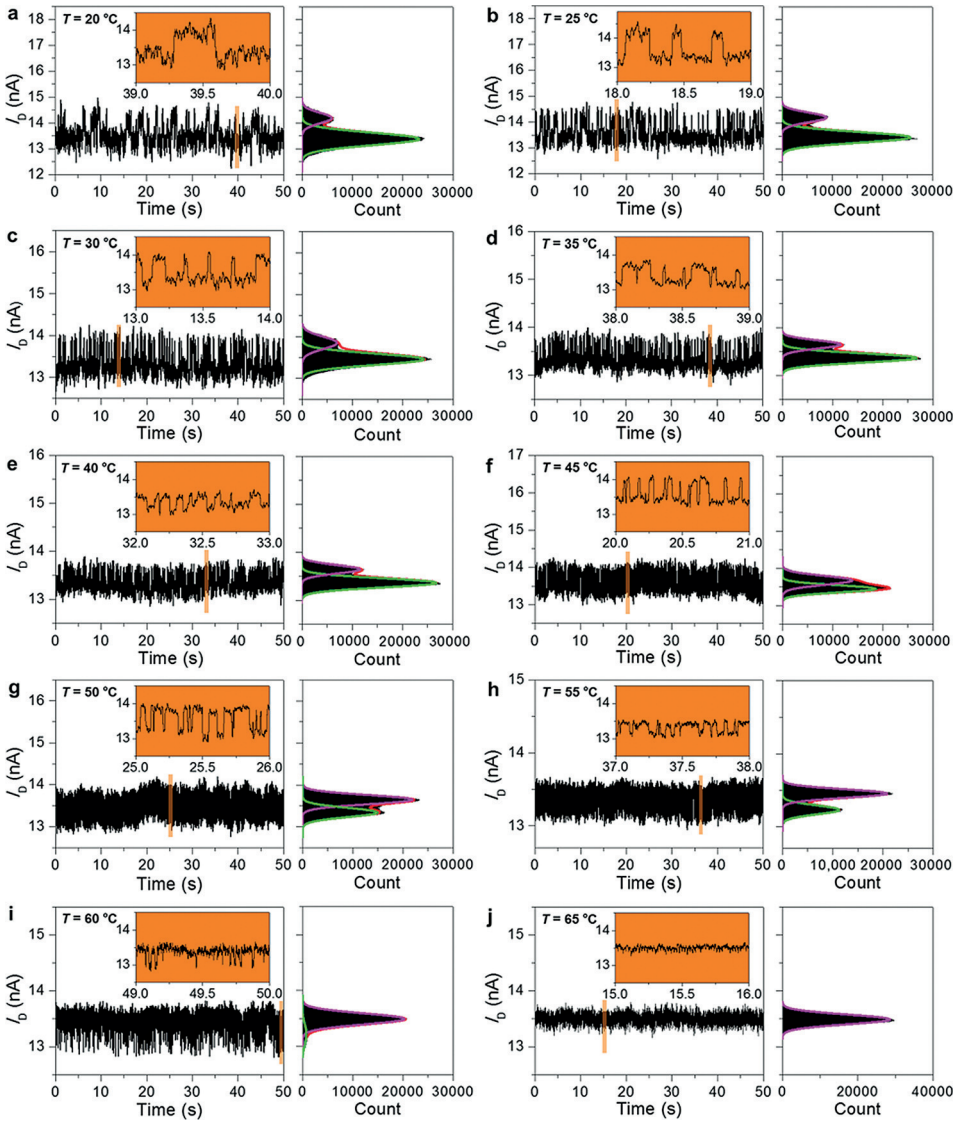


***Figure 2.*** Temperature dependence of hairpin DNA hybridization. These graphs show time-averaged data sets of a representative single-hairpin DNA-decorated SiNW biosensor (Device 1) measured in a PBS buffer solution at ten different temperatures varying from 20 °C to 65 °C (a: 20 °C; b: 25 °C; c: 30 °C; d: 35 °C; e: 40 °C; f: 45 °C; g: 50 °C; h: 55 °C; i: 60 °C; j: 65 °C). The left panels of each graph are real-time current recordings for a duration of 50 s. The inserts are the amplified 1-s data (yellow). The right panels are the corresponding histograms of the conductance for 200 s-interval data.

$\approx 182.57\ J\,K^{-1}\,mol^{-1}$. In comparison with previous reports using fluorescent methods ($\Delta H_m = 65 \pm 7\ kJ\,mol^{-1}$ and $\Delta S_m = 224 \pm 21\ J\,K^{-1}\,mol^{-1}$),[18] the values of the thermodynamic parameters we measured are in the same order of magnitude. However, a small difference originates from the strong dependence on stem/loop length and sequences, as well as metal ions in solution.[19] These values led to the negative free energies ($\Delta G_m$) of duplex dissociation above the $T_m$ and the positive free energies below the $T_m$, which is consistent with the experimental result that the single-stranded (high-conductance) conformation predominates above $T_m$ while the hairpin (low-conductance) conformation predominates below $T_m$.

To study the kinetics of hairpin DNA hybridization, we idealized thousands of current oscillations using a QUB software that is widely applied to deal with smFRET experiments in ion channels, and then extracted the lifetimes from the dwell-time histograms (Figure 3b).[20] Figure 3c and Figure S8 reveal that the dwell-time histograms of the high and low states can be well fit to a single-exponential decay function with the time constants $\tau_{high}$ and $\tau_{low}$, respectively. Accordingly, we found the hybridizing rate ($k_h$) using $k_h = 1/\tau_{high}$ and the melting rate ($k_m$) using $k_m = 1/\tau_{low}$, generating the Arrhenius plots (Figure 3d). The detailed kinetic results, including lifetimes and rates, are listed in Table S2. The Arrhenius plot of $k_m$ can be fit into a line with a positive activation energy ($E_m \approx 71.52\ kJ\,mol^{-1}$), indicating that the melting process follows an Arrhenius-like behavior and is strongly dependent on temperature. In good contrast, the plot of $k_h$ exhibits a sharp transition point around $T_m$, showing a positive activation energy in the low-temperature region ($E_{h1} \approx 67.03\ kJ\,mol^{-1}$) and a negative activation energy in the high-temperature region ($E_{h2} \approx -186.70\ kJ\,mol^{-1}$). This non-Arrhenius behavior, akin to protein folding,[21] demonstrates that hairpin DNA folding is dominated by enthalpy at low temperatures and by entropy at high temperatures, which is consistent with the previous report.[19]

To gain further insights into the kinetics of hairpin folding/unfolding at the single-molecule level, we calculated the normalized variance $r$ of $\tau_{high}$ and $\tau_{low}$ from the long-duration data sets through the formula:

$$r = \frac{\sigma^2}{<<\tau>>^2} = \frac{\sum_i (\tau_i - <<\tau>>)^2}{\sum_i \tau_i^2}$$

which is usually used to evaluate whether there exists hidden intermediate conformations in single-molecule dynamics studies. Any single-step Poisson process has a statistical variance $\sigma^2 = <\tau>^2$, namely $r = 1$.[22] As shown in Table S2, variances of both $\tau_{high}$ and $\tau_{low}$ at all different temperatures are much less than 1, implying that the folding/unfolding process of hairpin DNAs is not a simple single-step process and does

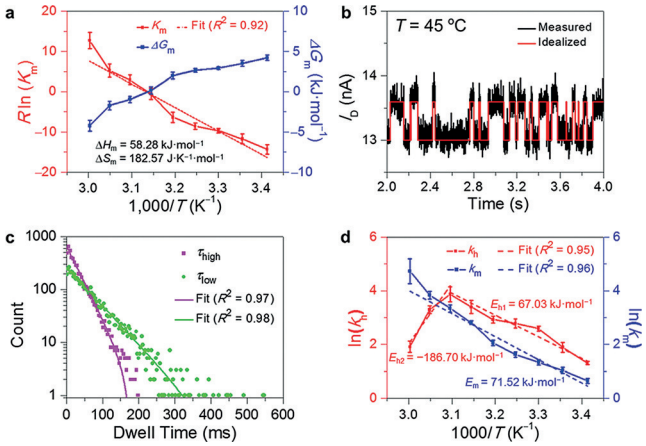


***Figure 3.*** a) Plots of $R\ln(K)$ (red) and Gibbs free energy (blue) to 1000/$T$ according to the thermodynamic relation. The red plot can be fitted with a line, whose slope is equal to the negative value of the enthalpy $\Delta H_m$ and the intercept is equal to the entropy $\Delta S_m$. b) Experimental data (black) of Device 1 measured at $T = 45\,°C$ and idealized data fitted by a QUB software (red). c) Dwell-time histograms of the high and low states in (b), showing single exponential decay fits with the lifetimes ($\tau_{high}$ and $\tau_{low}$). d) Arrhenius plots of hybridization (red) and dehybridization (blue) of a hairpin DNA, indicating non-Arrhenius and Arrhenius-like behaviors for the folding and unfolding processes, respectively. Error bars for (a) and (d) were calculated from two-level fluctuating data sets of five different devices.

possess hidden intermediates, which encouraged our further investigations as follows.

As previous studies reported that the base-by-base process of DNA hybridization could be captured at temperatures far below the melting point,[23] we focused our studies on the growing and declining regions of every current oscillation tested at 20 °C, and occasionally observed stepwise current increases and decreases that were clearly distinguishable from the random 1/$f$ noise (Figure 4a). Then, we fitted the data by using a step-finding algorithm and found that the growth and shrinkage can be fit into one to five steps (Figure 4a),[24] indicating multiple pathways in a single unfolding or folding process. In addition, the step-number histograms in Figure 4b extracted from thousands of oscillating events display a normal distribution where the three-step process is dominant in both the folding and unfolding processes. Considering the base pair number in the hairpin stem, we attribute the five-layer staircases in increases and decreases of electrical signals to the changes in the transmission probability at the single defect of silicon nanowires caused by the single base-pair dissociation and formation, respectively.

Generally, DNA hybridization obeys a kinetic zipper model, where a collapsing[25] and "fraying and peeling"[26] mechanism is predominant in duplex formation and dissociation, respectively. In our current case, we associated the zipper model with the stepwise growing and declining data, and then proposed a base-by-base, bottom-up unfolding/folding process (Figure 4c). The five base pairs in the hairpin stem are unwound or wound in a base-by-base manner, creating a five-step process. Because of the relatively weaker hydrogen bonds in A–T than in G–C, one or both of the A–T base pairs in the stem are likely to be unwound or wound along with the neighboring G–C base pairs, which results in a four-step or three-step process, respectively. In addition, a minor fraction of hairpin stems are stretched or folded in two patterns or in whole, producing conductance increases and decreases with only a plateau or no detectable pause. The base-by-base zipper model is further supported by the observation of the reverse steps in both the growing and declining processes (Figure S9), indicating rebinding or reopening/misfolding behaviors existing in the hairpin opening and closing processes.[27]

To acquire the kinetics of single base-pair hybridization/dehybridization, we only analyzed the successive, five-step events without consideration of backward behaviors. Figures 4d and 4f present a set of representative growing and declining data. According to the above-proposed zipper model, each step represents a base-pair dissociation or formation, and the duration of each plateau corresponds to

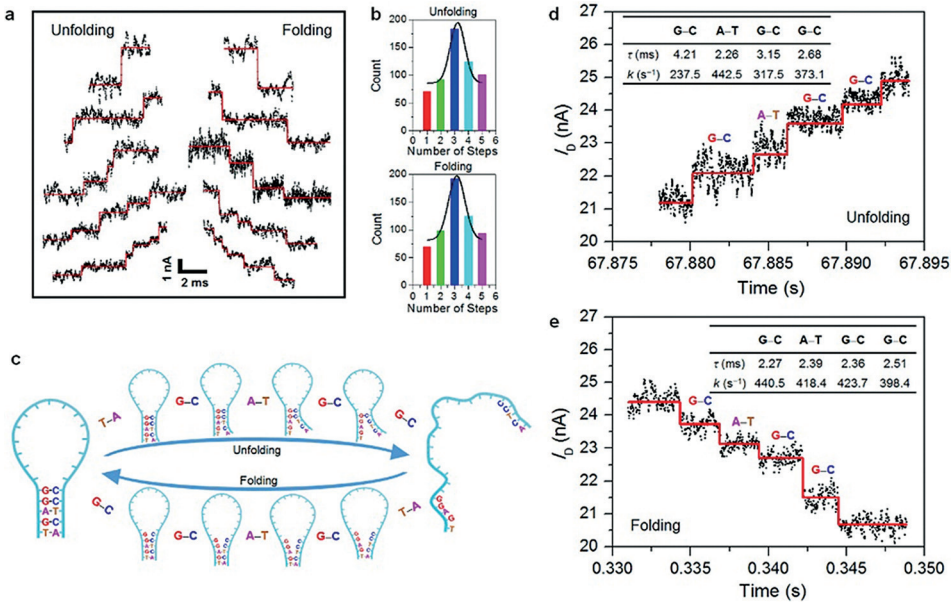


***Figure 4.*** a) Stepwise increases and decreases in conductance fitted by a step-finding algorithm (red), showing the zero- to five-step growing and declining processes. b) Histograms of the step numbers in growing (above) and declining (bottom) data counted from thousands of current oscillating events. c) The kinetic zipper model for the unfolding and folding processes of a hairpin DNA with five base pairs in stem. d–e) Representative five-step increasing and decreasing data of Device 3. The inserts show the possible microstates of each plateau (G–C, A–T, G–C, and G–C) and corresponding kinetic parameters (lifetime $\tau$ and rate $k$).

the lifetime of the preparation for unwinding or winding G–C, A–T, G–C, and G–C base pairs, respectively. We extracted the lifetime of each microstate from the dwell-time histograms of each plateau, which are well fit to a single-exponential decay function (Figure S10). As demonstrated in the insets of Figures 4 d and 4 e, the unwinding and winding rates of single base pair are on the submillisecond timescale, consistent with previous predictions.[4] We also found that the unfolding process is dependent on base sequences while the folding process is not. For the unfolding process, the lifetime of each plateau is not identical. The unzipping duration of the first G–C is the longest, followed by the second G–C, and then the third G–C. The unzipping time of A–T is the shortest. We attribute this difference to the strength of hydrogen bonds and the surface tension. First, hydrogen bonds in an A–T base pair are weaker than those in a G–C base pair because an A–T base pair possesses fewer hydrogen bonds, so unzipping A–T is the easiest. Second, when most base pairs are unwound, the ajar states bear much more tension than the former conformations. Therefore, the following G–C is more easily stretched than the foregoing G–C. Regarding the folding process, which undergoes a complicated pathway consisting of three elementary motions: end-to-end collisions, nucleation, and elongation of base-pairing,[28] the rate-determining step is the initial end-to-end collision of two stalks of the stem, whereas the following nucleation and elongation of base-pairing are accomplished in a successive, sequence-independent process.[29]

In summary, we demonstrated a label-free single-molecule detection system capable of detecting stochastic fluctuations under equilibrium conditions and time-dependent pathways of individual binding events in nonequilibrated systems on the submicrosecond timescale. By using this method, we successfully revealed single-molecule hairpin-DNA hybridization dynamics with single-base resolution. Without problems from photobleaching and fluorescent labeling, this methodology offers a platform for scientists to study fast single-molecule/single-event dynamics in an interdisciplinary realm, which is invaluable for the immediate investigation of many applications, such as genic polymorphism, protein folding, enzymatic activity, and reaction mechanisms.

## Acknowledgements

We acknowledge primary financial support from NSFC (21225311, 91333102, 21373014, and 21571021), and the 973 Project (2012CB921404).

**Keywords:** DNA hybridization · single-base resolution · single-molecule devices

**How to cite:** *Angew. Chem. Int. Ed.* **2016**, *55*, 9036–9040
*Angew. Chem.* **2016**, *128*, 9182–9186

[1] a) M. D. Baaske, M. R. Foreman, F. Vollmer, *Nat. Nanotechnol.* **2014**, *9*, 933–939; b) X. Zhuang, H. Kim, M. J. B. Pereira, H. P. Babcock, N. G. Walter, S. Chu, *Science* **2002**, *296*, 1473–1476.
[2] K. C. Neuman, A. Nagy, *Nat. Methods* **2008**, *5*, 491–505.
[3] a) Y. Choi, I. S. Moody, P. C. Sims, S. R. Hunt, B. L. Corso, I. Perez, G. A. Weiss, P. G. Collins, *Science* **2012**, *335*, 319–324; b) S. Sorgenfrei, C. – *y.* Chiu, R. L. Gonzalez, Y.-J. Yu, P. Kim, C. Nuckolls, K. L. Shepard, *Nat. Nanotechnol.* **2011**, 6, 126–132; c) C. Jia, B. Ma, N. Xin, X. Guo, *Acc. Chem. Res.* **2015**, *48*, 2565–2575.
[4] Y. Yin, X. S. Zhao, *Acc. Chem. Res.* **2011**, *44*, 1172–1181.
[5] X. Dai, M. B. Greizerstein, K. Nadas-Chinni, L. B. Rothman-Denes, *Proc. Natl. Acad. Sci. USA* **1997**, *94*, 2174–2179.
[6] R. Tsukanov, T. E. Tomov, M. Liber, Y. Berger, E. Nir, *Acc. Chem. Res.* **2014**, *47*, 1789–1798.
[7] H. Li, X. Ren, L. Ying, S. Balasubramanian, D. Klenerman, *Proc. Natl. Acad. Sci. USA* **2004**, *101*, 14425–14430.
[8] M. T. Woodside, W. M. Behnke-Parks, K. Larizadeh, K. Travers, D. Herschlag, S. M. Block, *Proc. Natl. Acad. Sci. USA* **2006**, *103*, 6190–6195.
[9] M. E. Polinkovsky, Y. Gambin, P. R. Banerjee, M. J. Erickstad, A. Groisman, A. A. Deniz, *Nat. Commun.* **2014**, *5*, 5737.
[10] F. Patolsky, G. Zheng, C. M. Lieber, *Anal. Chem.* **2006**, *78*, 4260–4269.
[11] J. Wang, F. Shen, Z. Wang, G. He, J. Qin, N. Cheng, M. Yao, L. Li, X. Guo, *Angew. Chem. Int. Ed.* **2014**, *53*, 5038–5043; *Angew. Chem.* **2014**, *126*, 5138–5143.
[12] H. Liang, X.-B. Zhang, Y. Lv, L. Gong, R. Wang, X. Zhu, R. Yang, W. Tan, *Acc. Chem. Res.* **2014**, *47*, 1891–1901.
[13] P. W. K. Rothemund, *Nature* **2006**, *440*, 297–302.
[14] B. M. Venkatesan, R. Bashir, *Nat. Nanotechnol.* **2011**, *6*, 615–624.
[15] P. M. Vallone, A. S. Benight, *Nucleic Acids Res.* **1999**, *27*, 3589–3596.
[16] Z. Li, Y. Chen, X. Li, T. I. Kamins, K. Nauka, R. S. Williams, *Nano Lett.* **2004**, *4*, 245–247.
[17] F. Patolsky, G. Zheng, O. Hayden, M. Lakadamyali, X. Zhuang, C. M. Lieber, *Proc. Natl. Acad. Sci. USA* **2004**, *101*, 14017–14022.
[18] G. Bonnet, S. Tyagi, A. Libchaber, F. R. Kramer, *Proc. Natl. Acad. Sci. USA* **1999**, *96*, 6171–6176.
[19] M. I. Wallace, L. Ying, S. Balasubramanian, D. Klenerman, *Proc. Natl. Acad. Sci. USA* **2001**, *98*, 5584–5589.
[20] C. Nicolai, F. Sachs, *Biophys. Rev. Lett.* **2013**, *08*, 191–211.
[21] P. Ferrara, J. Apostolakis, A. Caflisch, *J. Phys. Chem. B* **2000**, *104*, 5000–5010.
[22] W. Xu, J. S. Kong, P. Chen, *J. Phys. Chem. C* **2009**, *113*, 2393–2404.
[23] X. Chen, Y. Zhou, P. Qu, X. S. Zhao, *J. Am. Chem. Soc.* **2008**, *130*, 16947–16952.
[24] J. W. J. Kerssemakers, E. L. Munteanu, L. Laan, T. L. Noetzel, M. E. Janson, M. Dogterom, *Nature* **2006**, *442*, 709–712.
[25] H. Ma, C. Wan, A. Wu, A. H. Zewail, *Proc. Natl. Acad. Sci. USA* **2007**, *104*, 712–716.
[26] D. Andreatta, S. Sen, J. L. Pérez Lustres, S. A. Kovalenko, N. P. Ernsting, C. J. Murphy, R. S. Coleman, M. A. Berg, *J. Am. Chem. Soc.* **2006**, *128*, 6885–6892.
[27] G. R. Bowman, X. Huang, Y. Yao, J. Sun, G. Carlsson, L. J. Guibas, V. S. Pande, *J. Am. Chem. Soc.* **2008**, *130*, 9676–9678.
[28] J. Kim, S. Doose, H. Neuweiler, M. Sauer, *Nucleic Acids Res.* **2006**, *34*, 2516–2527.
[29] R. Tsukanov, T. E. Tomov, R. Masoud, H. Drory, N. Plavner, M. Liber, E. Nir, *J. Phys. Chem. B* **2013**, *117*, 11932–11942.

Received: March 28, 2016
Revised: May 8, 2016
Published online: June 8, 2016

  